ACS Electrochemistry

pubs.acs.org/electrochem

Article

Real-Time Detection and Quantification of Gaseous Products in a GDE Setup: CO_2 to Ethylene

Urban Sajevic, Walter A. Parada, Daniel M. Rottmann, Karl J. J. Mayrhofer, and Pavlo Nikolaienko*

Cite This: *ACS Electrochem.* 2025, 1, 2024−2033

Read Online

ACCESS | Metrics & More | Article Recommendations | Supporting Information

ABSTRACT: The electrochemical carbon dioxide reduction reaction (CO_2RR) is gaining significant attention as a promising solution to convert carbon emissions and intermittent solar and wind electricity into value-added building block chemicals and fuels. While advanced approaches such as gas diffusion electrodes (GDE) have achieved economically relevant reaction rates (>500 mA/cm^2), they unfortunately exhibit poor long-term stability, which is preventing industrial-scale CO_2RR implementation. We report a novel analytical setup that utilizes a parallel configuration of mass spectrometry and gas chromatography to enable accurate detection and quantification of major CO_2RR gaseous products at industrially relevant partial current densities (>200 mA/cm^2). The achieved sub-second resolution allows us to fully evaluate catalytic materials in extremely short time frames (<10 min) as well as reliably monitor product distribution shifts under intrinsic and induced dynamic conditions. Ultimately, this work presents a powerful tool that can help understand the intrinsic limitations of the GDE approach as well as drive the development of more efficient and stable electrolysis systems for the CO_2RR and similar processes.

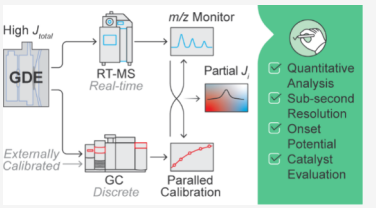

KEYWORDS: *CO_2RR, GDE, Real-time, Quantitative analysis*

INTRODUCTION

As concerns over the greenhouse effect and its contribution to climate change continue to escalate, it is becoming increasingly clear that mitigating further carbon dioxide (CO_2) discharge is key to achieving long-term sustainability.[1−3] Since CO_2 emissions are unavoidable in many essential industries,[4−6] developing effective technologies for their capture and utilization has become imperative.[7−10] Among such techniques, the electrochemical CO_2 reduction reaction (CO_2RR) has garnered significant attention.[11−13] It can harness renewable, but intermittent, solar and wind electricity[14−16] to repurpose the unwanted greenhouse gas as feedstock for producing value-added building block chemicals and fuels,[17−19] which are traditionally derived through energy-intensive, fossil-based petrochemical cracking.[20]

The product distribution of the CO_2RR can vary significantly depending on the electrocatalytic material used, as it is directly influenced by the binding energy of the absorbed reaction intermediates (CO* and H*) to the catalyst active sites.[21] If the CO* intermediate binds too strongly (e.g., Pt, Ni, Fe), the catalytic surface can become poisoned, resulting in the exclusive hydrogen evolution reaction (HER).[22] Conversely, weak interactions can cause premature detachment, resulting in the evolution of suboptimal CO (Ag, Au)[23−25] and HCOOH (Cd, Pb).[26] In this context, copper-based (Cu) catalysts have attracted the most attention, due to their unique combination of intermediate binding strengths, which enable the production of energy-dense multi-carbon (C_{2+}) products.[27,28]

The CO_2RR production rates, typically characterized by partial current densities, are highly dependent on reactant concentration[29,30] and are therefore heavily limited by the low solubility of CO_2 in aqueous electrolytes.[31] To increase the flux of CO_2 towards the catalytic surface and circumvent these mass transport limitations, a gas diffusion electrode (GDE) approach has been developed and widely adopted by the community.[32] Copper-based GDE configurations (Cu-GDE) can achieve a competitive partial current density ($j_{C_2H_4}$ > 200 mA/cm^2),[33] which provides the basis for the process's economic viability.[34] The latter is, however, yet to be fully achieved in large-scale industrial operations, as such electrolyzers remain limited by their poor long-term stability. To the best of our knowledge, even the most impressive CO_2-to-ethylene electrolyzers exhibit operation times under 300 h,[35−37] which is far from the required 35,000 h[38] that would ensure profitability, broad applicability, and consequently a real impact on CO_2 emission mitigation. The limitation is typically attributed to two primary deactivation mechanisms: intrinsic catalyst degradation and GDE electrowetting. While the former is well-researched[39] and can be mitigated through efficient catalyst design,[40,41] the latter remains unresolved.[42]

Received: April 2, 2025
Revised: July 12, 2025
Accepted: July 14, 2025
Published: July 28, 2025

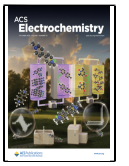

Since transformation of CO_2 into hydrocarbons includes a protonation step, a hydrogen source is required.[43] In the case of aqueous electrolytes, this condition is met by consumption of water molecules, which inevitably leads to an increase in local pH.[44] Although this benefits the selectivity,[45] it also enhances the concentration of carbonate ions (CO_3^{2-}) that form in the presence of continuously supplied CO_2.[46] Since the Helmholtz double layer consists predominantly of positively charged alkali cations (e.g., K^+), both ions combine to form carbonates, the concentration of which eventually reaches saturation values.[47] As a result, salt precipitation on the catalytic surface reduces the hydrophobicity of GDE, pushing the triple-phase boundary deeper in the GDE[42] and blocking its pores with aqueous electrolyte. Consequently, the reactant CO_2 must diffuse through the electrolyte to reach the active sites, which makes the CO_2RR mass transport limited and compromises the benefits of the GDE approach.[48]

Electrowetting-based deactivation of GDE can be further accelerated by activity-enhancing factors, such as high bulk pH and cation concentration and increased applied current density. Under extreme conditions it can occur in less than one h of operation. It can also be identified visually; however, this often requires a laborious and disruptive disassembly of the flow cell since the CO_2-supplying flow-field compartment is typically fabricated out of graphite to double as a current collector. A more practical approach is to monitor this deactivation phenomenon through a shift in product distribution from the CO_2RR toward the parasitic HER.[48] Therefore, developing and employing a reliable analytical system capable of accurately quantifying major CO_2RR products is essential. Although "in-line" gas chromatography (GC) configurations are a well-established solution for product analysis in long-term operations,[49] fast GDE deactivation can render them non-informative due to the limited time resolution imposed by the duration of the separation method. Therefore, to gain valuable insights into the rapid electrowetting mechanism, a much faster analytical method is required. The challenge has been previously addressed by coupling model catalytic systems with various real-time mass spectrometry (RT-MS) analyzers, which successfully enables the observation of time-dependent CO_2RR product evolution with sub-second resolution.[50−60] More recently, real-time product monitoring was also achieved in GDE-based electrolyzers, by installing capillary inlets near the electrode surface further advancing the state of the art.[61−65] These combined efforts have generated valuable insights into CO_2RR dynamics,[54] elucidating reaction pathways,[61,62] enabling rapid screening of catalytic materials,[60] and even identified products that are only produced in trace amounts.[65] However, despite the impressive advancements in the field, quantifying the m/z ratio signals and reliably detecting products at high current densities (>100 mA/cm^2) remain difficult, due to the differential sampling[66] approach and harsh local conditions such as bubble formation. This underscores the need for an optimized analytical system capable of detecting and accurately quantifying the main gaseous CO_2RR products at industrially relevant production rates while maintaining high temporal resolution.

In this work, we present an analytical setup that combines direct mass spectrometry and gas chromatography in a parallel configuration. This system enables real-time qualitative monitoring of the selected *m/z* ratios, while also allowing for their quantification against the pre-calibrated GC. By introducing the product stream from our custom Cu-GDE-based CO_2 electrolyzer into this analytical setup, we are able to 1) detect main descriptive CO_2RR (C_2H_4 and CH_4) and HER (H_2) products with sub-second resolution; 2) accurately quantify the production rates of observed products across various reaction conditions and over extended time frames; 3) cover an industrially relevant range of production rates (>100 mA/cm^2); 4) fully evaluate catalytic materials with key performance factors such as onset potentials, activity descriptors, and product distribution shifts under dynamic electrochemical conditions in a previously unachieved time range (<10 min). More importantly, we also gain valuable insights into these factors during the GDE's intrinsic electrowetting and subsequent deactivation phenomenon, providing a useful tool for knowledge-driven development of novel designs and configurations for long-term operating GDEs in the CO_2RR and beyond.

EXPERIMENTAL METHODS

Cell Preparation. The electrochemical measurements demonstrated in this study are performed in a custom-designed three electrode PTFE flow (Figure 1) cell controlled

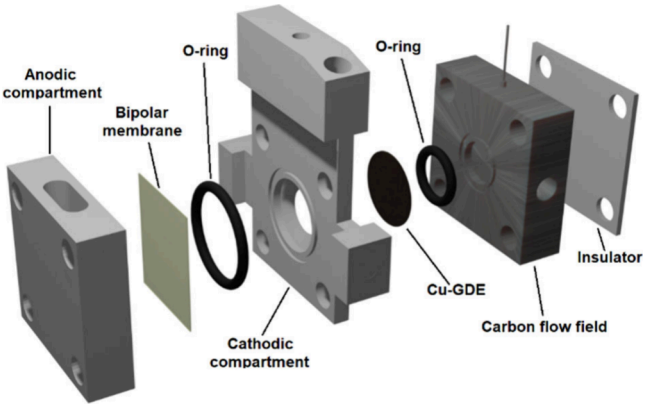

Figure 1. An exploded view of the in-house developed three-electrode GDE flow cell[68] used in this study.

by a Biologic SP 240 potentiostat, additionally equipped with a 4 A (−3, 10 V) booster channel. The cell is fitted with a 6 mm Hg/HgO reference electrode (BASi), Ir-MMO counter electrode mesh (Metakem), and a bipolar membrane (FUMASEP), which separates the cathodic and anodic compartments and prevents product crossover.[67] The cathodic compartment holds 12 mL of the electrolyte that is recirculated by a peristaltic pump (Reglo ICC ISMATEC) with a constant flow of 5 mL min^{-1}. It is designed to limit the working GDE's active area to 1 cm^2, with a tilt above the electrode that allows efficient transport of formed bubbles to the integrated compartment's headspace. The latter serves as a volume for the recombination of gaseous products from both sides of the GDE and their subsequent analysis and quantification. The carbon flow-field that contacts the GDE is purged with a constant flow of CO_2 (20 mL/min). To prevent damaging the catalyst layer due to excessive gas flow through the GDE, a tube connects the flow-field to the cathodic compartment's headspace, recombining the excess CO_2 (and gases produced at the GDE's backside) with the main gaseous products.

To prepare the copper gas diffusion electrodes (Cu-GDE), 50 mg of a Nafion solution (20 wt %, Sigma-Aldrich) and 90

https://doi.org/10.1021/acselectrochem.5c00130
ACS Electrochem. 2025, 1, 2024−2033

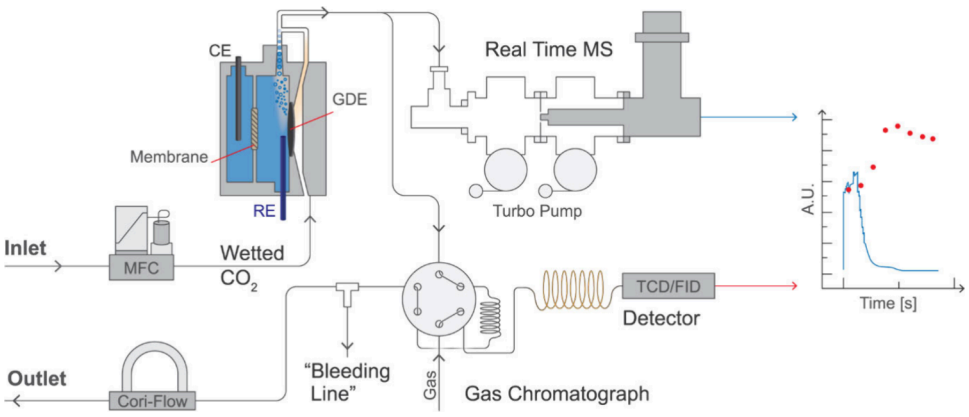

Figure 2. Schematic representation of the analytical setup with MS and GC in a parallel configuration, connected to a custom developed GDE flow cell.

mg of CuNP (25 nm, Sigma-Aldrich) are mixed in 2500 mg of 2-propanol. The solution is then treated with an ultrasonification horn (SFX 150, Branson) at 30% intensity for a total time of 15 min, consisting of sequential 3 s pulses and 2 s pauses. The obtained ink is spray-coated on a PTFE treated carbon gas diffusion layer (33 mm·30 mm, Freudenberg H23C8) until a catalyst loading of 1 mg/cm^2 is achieved. A circular area with a diameter of 26 mm is punched out and utilized as the Cu-GDE.

The electrolytes for this work are prepared in ultrapure water (Milli-Q IQ 7000, Merck). The pH value of 14 is achieved by preparing a 1 M KOH (pellets, 99.99%, Sigma-Aldrich) solution. For pH 9, we prepare 1 L of a buffered solution by combining 50.06 g of $KHCO_3$ (99.95%, Sigma-Aldrich) and 34.55 g of K_2CO_3 (99.99%, Sigma-Aldrich). For the last electrolyte, we prepare a 1 M KOH solution and acidify it with H_3PO_4, until a pH value of 3 is reached. All three electrolytes are designed to minimize the influence of anions and focus solely on the pH effect. The electrolytes with pH 9 and 14 were chosen based on the fact that in contact with CO_2, KOH forms CO_3^{2-}/HCO_3^- anions. For pH 3, H_3PO_4 was chosen as the acidifying agent, due to the fact that among all the inorganic acids, the PO_4^{3-} anion exhibits the smallest influence on the CO_2RR performance.

Gas Analysis. We present the configuration of our gas analysis setup in Figure 2. After recombination in the cathodic compartment's headspace, the product stream exits the cell through tube, which has an inside diameter (ID) of 3 mm. The volumetric flow of the product stream is quantified by an in-line Coriolis mass flow meter (mini-CORI-FLOW M13, Bronkhorst), while the temperature and pressure are monitored by an in-line pressure gauge (DM01, BDSolutions). Throughout all of the experiments, the volumetric flow of the product stream remained between 18 and 22 mL/min. In this range, no pressure fluctuations within the product stream could be detected, with the measured pressure relative to the atmosphere remaining constant (p_0 = 13 mbar). An oversight of these parameters throughout operation guarantees analytical accuracy despite the changes induced by the shift in the CO_2RR product distribution.

The product stream is further directed into a GC (Clarus 580 with Arnel solution, Perkin Elmer), where the products are quantified. We utilize a chromatography method that is 13 min long and can accurately separate and quantify H_2, CO_2, C_2H_4, CH_4, and CO. Due to the nature of these gases, 2 columns are needed for efficient separation: a silica packed separation column and a mole sieve. As the latter must not be exposed to CO_2 to prevent poisoning, two different configuration modes are utilized at pre-determined time intervals (Figure S1). During sample injection and the following 6.5 min, Valve 1 operates in injection mode (Figure S1b) resulting in the sample loop being diverted to the column. Valve 2 ensures that no sample reaches the mole sieve column, and Valve 3 disconnects the methanizer-supported flame ionization detector (FID). In this mode, the CO_2RR product stream also bypasses the sample loop, which results in lower fluidic resistance and base pressure in the system (p_0 = 13 mbar). At 6.5 min, the GC returns into collection mode (Figure S1a), in which Valves 2 and 3 re-enable mole-sieve column and FID respectively. During this mode, the CO_2RR product stream again passes through the sample loop, which increases the fluidic resistance and consequently the pressure in the system by ∼45 mbar. The effect of these pressure shifts and their eventual removal are discussed further at the beginning of the Results and Discussion section. The evolved products are monitored with an FID and thermal conductivity detector (TCD), which are pre-calibrated with calibration mixtures of various analyte concentrations. The calibration mixes were prepared by diluting a commercially-supplied gas mixture that exhibits a high concentration of all four analytes (H_2, C_2H_4, CH_4, and CO) in the CO_2 matrix, with additional pure CO_2 gas, using a T-piece and mass flow controllers. Such a calibration procedure ensures reliable quantification of the GC signal over a broad concentration range, resulting in the ability to accurately assess the concentration, partial volumetric flow, and ultimately the partial current density of each analyte at the time of a GC injection.

To achieve sub-second time resolution of our analytical setup, we additionally connect the product stream exiting the cell to an electron impact quadrupole mass spectrometer (EI-QMS) (QMA 410 equipped with 90°-off-axis SEM 217 and crossbeam ion source, Pfeiffer Vacuum) in parallel. The connection is realized by an installed T-piece that introduces a 120 cm long PEK capillary with an ID of 150 μm. The capillary's dimensions ensure a low but very stable pressure of $3.63 \cdot 10^{-3}$ in the EI-QMS pre-chamber, which results in drawing a representative amount of sample without disrupting the main product stream flow. The pre-chamber is further connected to the main chamber with another capillary, resulting in the main chamber pressure stabilizing at 1.57·

https://doi.org/10.1021/acselectrochem.5c00130
ACS Electrochem. 2025, 1, 2024−2033

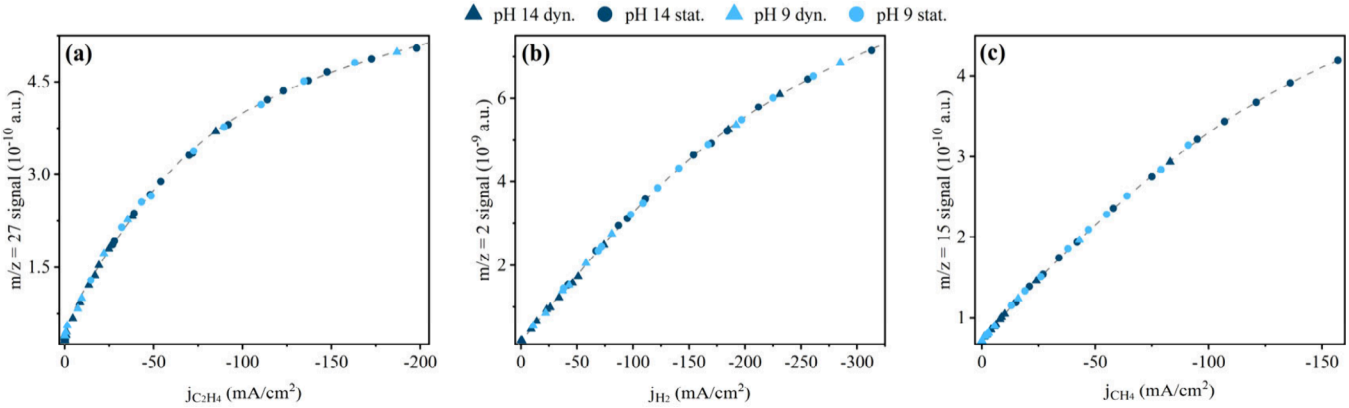

Figure 3. Polynomial (quartic) regression of the EI-QMS signals related to GC-derived partial current densities for (a) ethylene, (b) hydrogen, and (c) methane respectively, at the main-chamber pressure of $1.57 \cdot 10^{-7}$ bar.

10^{-7} bar. The described combination of low-volume connections and capillary sizes, coupled with an above-mentioned relatively high flow of supplied CO_2 (20 mL/min), ensures that the gases produced at the GDE's surface are promptly isolated and reproducibly transported to the MS. This was confirmed by conducting multiple start-of-electrolysis experiments, which resulted in a fixed MS response delay time of 8 s for Hydrogen and 12 s for Ethylene and Methane. All of the MS signals discussed in this work were therefore shifted by their respective delay time.

Inside the main chamber, the Iridium filament operates at the emission current of 0.5 A, a protective current of 4.2 A, and cathode voltage of −70 V. The signal is amplified by a secondary electron multiplier (SEM) operating at a constant voltage of 1550 V. The detector operates in the 10^{-5} A range with the resolution set to 98 and a dwell time of 200 ms for each observed m/z ratio. To observe hydrogen production, an m/z ratio of 2 was chosen. For ethylene and methane, we monitored the m/z values of 27 and 15 respectively. Those two values are associated with their first fragmentation cations and were chosen to prevent unwanted influence that would arrive at their main spectroscopic peaks (m/z 28 and 16) due to nitrogen and oxygen present in air. It is worth mentioning that we do not monitor the produced carbon monoxide, as the selected harsh ionization conditions cause fragmentation of the abundant CO_2 and consequential overlap of CO and CO_2 peaks. Despite the shared fragmentation pathways, the system could also enable quantification of CO's production rate of COs, however only by weakening the ionization strength, which would result in reduced accuracy at the upper detection limit for other, economically more significant products.

EI-QMS Quantification. With the goal of enabling real time quantification in our EI-QMS-GC setup, we define calibration curves for the main gaseous products, correlating the dimensionless m/z signals to their corresponding partial current densities (Figure 3). To ensure the reliability of such quantification across several reaction parameters, we conduct both static (CP) and dynamic (LSV) CO_2RR experiments in electrolytes with bulk pH values of 9 and 14.

The quantity of sample introduced to the EI-QMS ionization source, which is closely correlated with the pressure within the main chamber, directly affects the detector response and, consequently, the m/z signal. Since sample introduction is driven by a pressure differential between the product stream and the main EI-QMS chamber, it is inherently governed by the fluidic resistance of the capillary. Consequently, reliable quantification is possible only whenever the latter remains constant, which can be observed through a stable pressure reading for the EI-QMS main chamber. For this reason, we conduct the above-mentioned experiments over several working weeks, ensuring no time-dependent drift of the calibration factors, which could arise from capillary blockages. To quantify each data point, the exact time of GC injection is noted, and the GC-calculated value of partial current density is correlated to the corresponding m/z signal data point.

The calibration curves for all three products presented in Figure 3 can be well-defined with a quartic polynomial equation ($y = Ax^4 + Bx^3 + Cx^2 + Dx + E$, where y is $j_{partial}$ and x is the m/z signal), with A, B, C, D, and R^2 factors presented in Table S1. It is important to note the nonlinearity of the calibration curves, known as polynomial (quartic) regression, which is a well understood phenomenon in mass spectrometry.[69−71] At higher sample concentrations, the MS response can be inhibited due to various factors such as saturation of detector,[72] ion suppression,[74] decreased ionization efficiency, and matrix effects.[73] The latter two phenomena are particularly relevant for analytes with higher mass-to-charge ratios, as a larger molecular size increases the susceptibility to such interactions. This is also the case for our calibration curves, as the ethylene signal (m/z = 27) in Figure 3a exhibits the highest degree of regression, followed by methane (m/z = 15) (Figure 3c) and eventually the hydrogen signal (m/z = 2) (Figure 3b). Although nonlinear, the quartic calibration curves exhibit an impressive R^2 factor of >0.999 for all three products, supporting the reliability of our calibration and therefore the accuracy of our quantification method.[75,76] It is important to note that, while the partial current density ranges displayed in Figure 3 are directly relevant to our experimental requirements, the system's design also allows for the accurate detection of much higher partial current densities. This can be achieved by simply increasing the fluid resistance of the connecting capillary, either by extending its length or reducing its inner diameter, as described by Poiseuille's law. While such a change would necessitate a recalibration of the system, our integral method of sample collection allows our system to accurately quantify production in a >1 A partial current density range.

RESULTS AND DISCUSSION

To test the long-term stability of Cu-GDE samples at industrially relevant conditions, we perform the CO_2RR

https://doi.org/10.1021/acselectrochem.5c00130
ACS Electrochem. 2025, 1, 2024−2033

through chrono potentiometric (CP) measurements at −400 mA/cm^2 (Figure 4). If we describe the reaction performance solely through GC supported product analysis (Figure 4a), an unprecedented rapid GDE deactivation is observed. Monitoring the reaction with our real-time analytics unveils dire inconsistencies in the ethylene production signal. The positions of these unexpected features on the time axis reveal their connection to the moderate (∼45 mbar) pressure fluctuations,[77] which are inadvertently caused by GC switching operational modes, as explained in the Gas Analysis section. To remove these features, we install another T-piece just before the sample loop of the GC, where we connect a "bleeding line" capillary (ID = 80 μm), which was kept throughout all presented studies. The capillary length is designed to result in the exact fluid resistance that maintains a seal under constant operating conditions at pressure relative to atmosphere p_0 = 13 mbar but releases any excess pressure over that value that would otherwise be present during the sample collection mode. Conducting the CO_2RR via CP at −400 mA/cm^2 in the updated GC configuration proves the effectivity of the installed "bleeding line" by establishing isobaric conditions, which drastically prolong the Cu-GDE performance (Figure 4b), extending the time of high partial current density ethylene production (>100 mA/cm^2) from 1600 s to >6 h. The measured potential responses for this experiment are presented in Figure S3, further proving the early deactivation of the GDE is influenced by the pressure fluctuations.

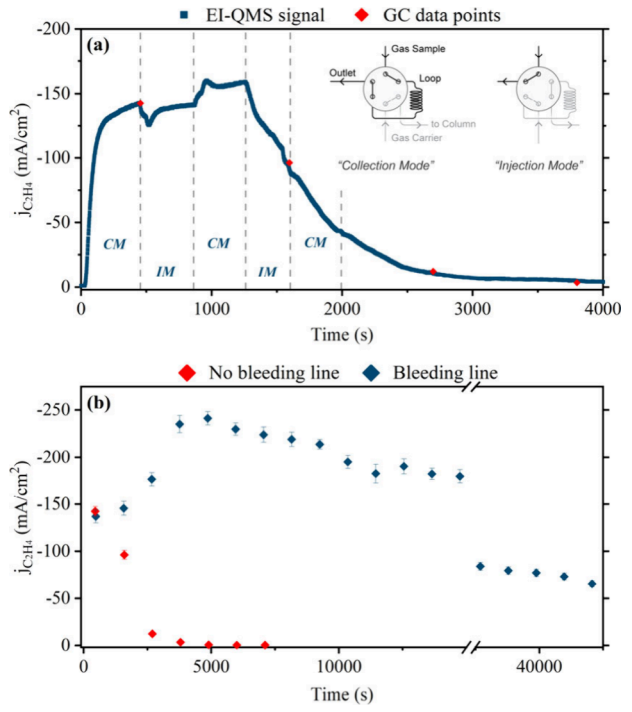

Figure 4. Long-term CO_2RR chronopotentiometry at −400 mA/cm^2 was monitored with EI-QMS and GC. (a) Relative pressure fluctuations induced by the GC switching between the collection mode (CM) and injection mode (IM) and their effect on $j_{C_2H_4}$. (b) Comparison of GC-monitored long-term performance with and without the installed "bleeding line".

To further test the versatility of our newly developed analytical setup, we perform the CO_2RR on Cu-GDE in three different electrolytes with pH values of 3, 9, and 14. This approach is not only useful to determine the accuracy of our setup across the pH spectra but also provides some insightful information about how the bulk electrolyte pH influences the CO_2RR dynamics. We focus solely on the effect of bulk pH and prevent any possible discrepancies due to the acknowledged cation effect,[78,79] by fixing the cation concentration to [K^+] = 1 M across all electrolytes and experiments, as described in the Cell Preparation section.

We first study how the bulk electrolyte pH affects the onset potentials of major gaseous products by conducting linear

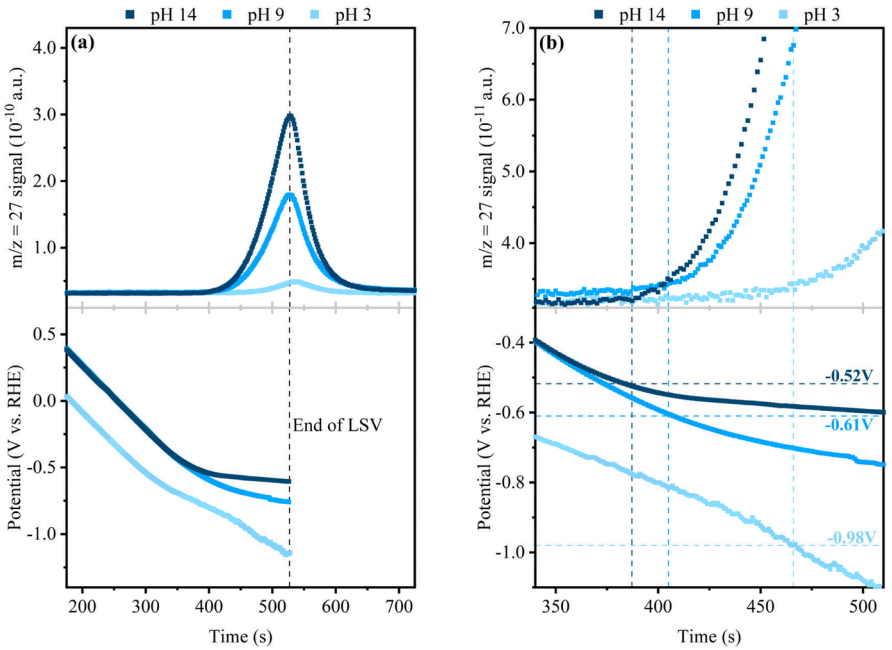

Figure 5. LSV experiments in electrolytes with three different bulk pH values. (a) EI-QMS signal for m/z = 27 (ethylene) and the measured potential vs. RHE. (b) Zoomed-in graph displaying the ethylene on-set potential values.

https://doi.org/10.1021/acselectrochem.5c00130
ACS Electrochem. 2025, 1, 2024−2033

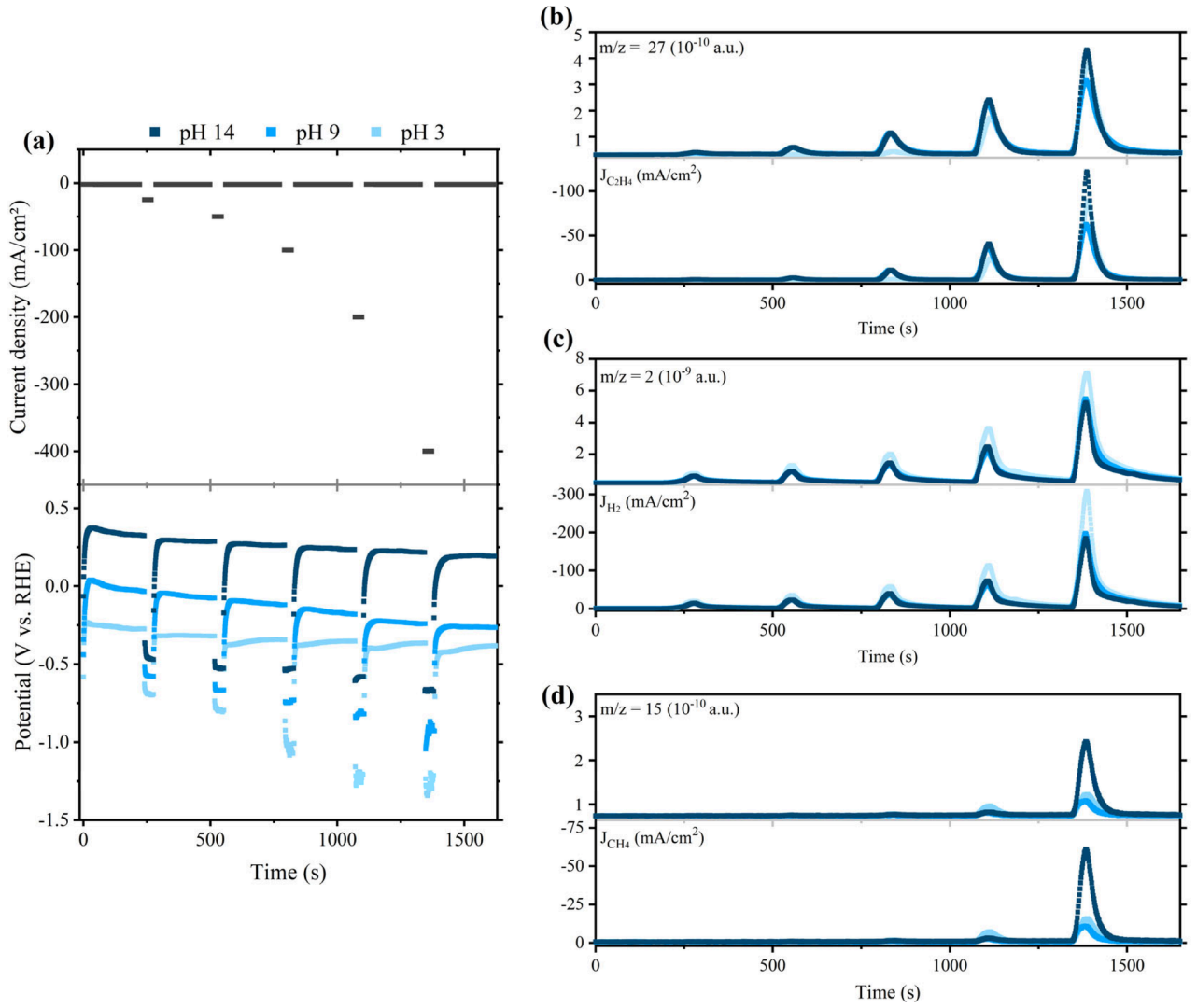

Figure 6. Chronopotentiometry and gEIS holds in electrolytes with three different bulk pH values. (a) The applied current density profile along with the RHE scale potential responses. (b-d) Corresponding EI-QMS signals of main gaseous CO_2RR products along with their derived partial current densities for (b) ethylene, (c) hydrogen, and (d) methane, respectively.

sweep voltammetry (LSV). To maximize the accuracy of acquired values, a moderate scan rate of 10 mV/s is applied, while the sample is pre-conditioned by conducting a CP at −1 mA/cm^2 for 150 seconds, which reduces any copper oxides that could have formed during exposure to air. As is evident in Figure 5, the onset potentials are determined by correlating each product's EI-QMS signal to the LSV graph. Since the beginning of production is characterized by an increase in the respective m/z signal, we determine the initial point of such an increase to be the first value that deviates from the pre-determined average baseline value by >2% and stays above this threshold for the duration of the scan.

Utilizing this approach, we successfully determine the on-set potential values of C_2H_4 for this Cu-GDE to be −0.98 V, −0.61 V, and −0.52 V (V vs. RHE) in the bulk electrolyte pH of 3, 9, and 14 respectively (Figure 5b). The same procedure is also applied to hydrogen- and methane-related signals to observe the corresponding on-set potentials (Table S2). The obtained values fall well in line with the consensus in the literature,[80,81] showcasing the precision of our setup.

To prove additional use cases, we continue experimentation in the same electrolyte conditions and observe the resulting CO_2RR product distribution trends. We deploy a dynamic electrochemical procedure, which focuses on obtaining performance descriptors in various operating conditions, in a short period of time − a feat unachievable with standard GC configurations. The procedure, showcased in Figure 6a, relies on 2 min steps of galvanostatic electrochemical impedance spectroscopy (gEIS), complete with intermediate "resting" periods. The gEIS steps were performed at −25, −50, −100, −200, and −400 mA/cm^2, with a 1% amplitude in current densities. Such a technique is favored over standardly applied CP steps due to the half-cell resistance depending heavily on the formation of liquid products[82] and protrusion of the electrolyte inside the GDE's pores. Such a gEIS approach allows us to track the development of half-cell resistance over the course of the experiment (Figure S2) and therefore accurately translate the measured potential to the RHE scale. During the resting periods, CP holds of −1 mA/cm^2 are applied, which not only prevents any copper oxidation associated with exposure to the OCP but also postpones possible deactivation of the Cu-GDE.

Comparing the RHE corrected potential response (Figure 6a) to the EI-QMS signal corresponding to evolution of

https://doi.org/10.1021/acselectrochem.5c00130
ACS Electrochem. 2025, 1, 2024−2033

gaseous products from Figure 6(b-d), we gain interesting insights into the CO_2RR behavior. We also successfully utilize the calibration equations from Figure 3 to quantify the EI-QMS signal toward time resolved partial current densities of the observed products, proving the applicability of our quantification technique. It is important to note that the duration of gEIS steps is fine-tuned through trial and error to the minimal time that still enables the m/z signal to reach the characteristic value. By doing that, we minimize the amount of charge passed through the Cu-GDE and prevent the unwanted negative impact on performance descriptors due to electrowetting-propagated electrode deactivation.

As displayed in Figure 6b, we confirm the field's consensus[83] that the production of ethylene is greatly enhanced in the highly alkaline environment, not only in terms of the production rate but also with regards to the required potential vs. RHE. A comparison with onset potential values from Table S2 shows that in high pH conditions, industrially relevant partial current densities of ethylene production ($j_{C_2H_4}$ > 50 mA/cm^2) are already possible when the applied potential is only 60 mV more negative than the on-set potential (−0.58 V compared to −0.52 V vs. RHE). For comparison, to obtain similar ethylene production in pH 9 and 3, this value must be increased to 190 and 220 mV respectively, which would drastically increase the operational costs of non-alkaline electrolyzers. The trend is also present within methane production, where a rather insignificant potential difference of 90 mV for pH 14 produces significantly more methane than the 130 and 240 mV potential differences for pH 9 and 3 respectively (Figure 6d). Contrary to the CO_2RR, the parasitic hydrogen evolution tends to be much more pronounced in acidic conditions (Figure 6c), which is to be expected due to a high concentration of available H^+ species. It is interesting to note that while strong alkaline conditions observe higher C_2H_4 and CH_4 production, the slight alkalinity of pH 9 is sufficient to prevent the presence of freely available H^+ species. This results in both pH values of 9 and 14 exhibiting almost identical HER performance. The missing part of partial current density for pH 9 can be attributed to CO formation, which is also well supported by the literature.[45] It is also interesting to point out that while the CO_2RR in acidic conditions can reach industrially relevant current densities, the associated high half-cell resistance drastically increases the required applied potential, greatly inhibiting the economic viability of such systems. Finally, we compare the overall production peaks to the potential responses on the RHE scale, confirming that whenever the onset potential for that product is not reached, there will also be no corresponding EI-QMS signal, solidifying the reliability and accuracy of our setup.

CONCLUSION

In summary, we present a novel GC supported mass spectrometry configuration that enables real time analysis and quantification of gaseous electrolysis products at industrially relevant current densities. To demonstrate its accuracy, we choose a complex multi-product CO_2RR, which we couple with the advanced and until now non-quantifiable GDE-based approach. Doing this, we highlight how our setup can provide some key descriptive parameters across various reaction conditions but, more importantly, is also able to track the product distribution shifts during both intrinsic and induced dynamic conditions. We are confident that the accessibility and reproducibility of our analytical setup will facilitate a more comprehensive understanding of the intrinsic GDE electrowetting phenomena as well as significantly contribute to advancements in related scientific fields.

ASSOCIATED CONTENT

Supporting Information

The Supporting Information is available free of charge at https://pubs.acs.org/doi/10.1021/acselectrochem.5c00130.

GC configurations, GC calibration data, dynamic experiment half-cell resistance evolution, measured potential responses of CP experiments, CO_2RR gaseous products associated onset potentials in different pH's (PDF)

AUTHOR INFORMATION

Corresponding Author

Pavlo Nikolaienko − *Helmholtz Institute Erlangen-Nürnberg for Renewable Energy (IET-2), Forschungszentrum Jülich GmbH, 91058 Erlangen, Germany;* orcid.org/0000-0002-1508-7589; Email: p.nikolaienko@fz-juelich.de

Authors

Urban Sajevic − *Helmholtz Institute Erlangen-Nürnberg for Renewable Energy (IET-2), Forschungszentrum Jülich GmbH, 91058 Erlangen, Germany;* orcid.org/0009-0009-8038-043X

Walter A. Parada − *Helmholtz Institute Erlangen-Nürnberg for Renewable Energy (IET-2), Forschungszentrum Jülich GmbH, 91058 Erlangen, Germany; Friedrich-Alexander-Universität Erlangen-Nürnberg, Department of Chemical and Biochemical Engineering, 91058 Erlangen, Germany;* orcid.org/0000-0002-5413-1917

Daniel M. Rottmann − *Friedrich-Alexander-Universität Erlangen-Nürnberg, Department of Chemical and Biochemical Engineering, 91058 Erlangen, Germany; Wacker Chemie AG, Consortium für Elektrochemische Industrie, 81379 Munich, Germany;* orcid.org/0009-0008-9991-3526

Karl J. J. Mayrhofer − *Helmholtz Institute Erlangen-Nürnberg for Renewable Energy (IET-2), Forschungszentrum Jülich GmbH, 91058 Erlangen, Germany; Friedrich-Alexander-Universität Erlangen-Nürnberg, Department of Chemical and Biochemical Engineering, 91058 Erlangen, Germany;* orcid.org/0000-0002-4248-0431

Complete contact information is available at: https://pubs.acs.org/10.1021/acselectrochem.5c00130

Author Contributions

U.S., P.N., and K.J.J.M. contributed to the manuscript's writing and topic conceptualization. U.S. and W.A.P. developed the real-time analytical system. U.S. performed electrochemical measurements, realized the quantification technique, and performed the data treatment. D.R. contributed to topic conceptualization and data evaluation.

Notes

The authors declare no competing financial interest.

ACKNOWLEDGMENTS

U.S. gratefully acknowledges Wacker Chemie AG for their financial support of this research.

REFERENCES

(1) Yoro, K. O.; Daramola, M. O. Chapter 1 - CO_2 emission sources, greenhouse gases, and the global warming effect. In *Advances in Carbon Capture*, Rahimpour, M. R., Farsi, M., Makarem, M. A., Eds.; Woodhead Publishing, 2020; pp 3−28.

(2) Centre, J. R.; Environment, I. f.; Sustainability; Agency, P. N. E. A.; Olivier, J.; Janssens-Maenhout, G.; Peters, J. *Trends in global CO_2 emissions − 2012 report*; Publications Office, 2012. https://doi.org/10.2788/33777.

(3) Solomon, S.; Plattner, G.-K.; Knutti, R.; Friedlingstein, P. Irreversible climate change due to carbon dioxide emissions. *Proc. Natl. Acad. Sci. U. S. A.* **2009**, *106* (6), 1704−1709.

(4) Worrell, E.; Price, L.; Martin, N.; Hendriks, C.; Meida, L. O. Carbon Dioxide Emmisions From The Global Cement Industry. *Annual Review of Environment and Resources* **2001**, *26* (1), 303−329.

(5) Ren, T.; Patel, M. K. Basic petrochemicals from natural gas, coal and biomass: Energy use and CO_2 emissions. *Resources, Conservation and Recycling* **2009**, *53* (9), 513−528.

(6) Solaymani, S. CO_2 emissions patterns in 7 top carbon emitter economies: The case of transport sector. *Energy* **2019**, *168*, 989−1001.

(7) Ostovari, H.; Müller, L.; Skocek, J.; Bardow, A. From Unavoidable CO_2 Source to CO_2 Sink? A Cement Industry Based on CO_2 Mineralization. *Environ. Sci. Technol.* **2021**, *55* (8), 5212−5223.

(8) Hepburn, C.; Adlen, E.; Beddington, J.; Carter, E. A.; Fuss, S.; Mac Dowell, N.; Minx, J. C.; Smith, P.; Williams, C. K. The technological and economic prospects for CO_2 utilization and removal. *Nature* **2019**, *575* (7781), 87−97.

(9) Huang, C.-H.; Tan, C.-S. A Review: CO_2 Utilization. *Aerosol and Air Quality Research* **2014**, *14* (2), 480−499.

(10) Artz, J.; Müller, T. E.; Thenert, K.; Kleinekorte, J.; Meys, R.; Sternberg, A.; Bardow, A.; Leitner, W. Sustainable Conversion of Carbon Dioxide: An Integrated Review of Catalysis and Life Cycle Assessment. *Chem. Rev.* **2018**, *118* (2), 434−504.

(11) Whipple, D. T.; Kenis, P. J. A. Prospects of CO_2 Utilization via Direct Heterogeneous Electrochemical Reduction. *J. Phys. Chem. Lett.* **2010**, *1* (24), 3451−3458.

(12) Sánchez, O. G.; Birdja, Y. Y.; Bulut, M.; Vaes, J.; Breugelmans, T.; Pant, D. Recent advances in industrial CO_2 electroreduction. *Current Opinion in Green and Sustainable Chemistry* **2019**, *16*, 47−56.

(13) Liu, M.; Pang, Y.; Zhang, B.; De Luna, P.; Voznyy, O.; Xu, J.; Zheng, X.; Dinh, C. T.; Fan, F.; Cao, C.; et al. Enhanced electrocatalytic CO_2 reduction via field-induced reagent concentration. *Nature* **2016**, *537* (7620), 382−386.

(14) Montoya, J. H.; Seitz, L. C.; Chakthranont, P.; Vojvodic, A.; Jaramillo, T. F.; Nørskov, J. K. Materials for solar fuels and chemicals. *Nature Materials* **2017**, *16* (1), 70−81.

(15) Bonke, S. A.; Wiechen, M.; MacFarlane, D. R.; Spiccia, L. Renewable fuels from concentrated solar power: towards practical artificial photosynthesis. *Energy Environ. Sci.* **2015**, *8* (9), 2791−2796.

(16) Chen, Z.; Jaramillo, T. F.; Deutsch, T. G.; Kleiman-Shwarsctein, A.; Forman, A. J.; Gaillard, N.; Garland, R.; Takanabe, K.; Heske, C.; Sunkara, M.; et al. Accelerating materials development for photoelectrochemical hydrogen production: Standards for methods, definitions, and reporting protocols. *Journal of Materials Research* **2010**, *25* (1), 3−16.

(17) Nielsen, D. U.; Hu, X.-M.; Daasbjerg, K.; Skrydstrup, T. Chemically and electrochemically catalysed conversion of CO_2 to CO with follow-up utilization to value-added chemicals. *Nature Catalysis* **2018**, *1* (4), 244−254.

(18) Zhu, P.; Wang, H. High-purity and high-concentration liquid fuels through CO_2 electroreduction. *Nature Catalysis* **2021**, *4* (11), 943−951.

(19) De Luna, P.; Hahn, C.; Higgins, D.; Jaffer, S. A.; Jaramillo, T. F.; Sargent, E. H. What would it take for renewably powered electrosynthesis to displace petrochemical processes? *Science* **2019**, *364* (6438), No. eaav3506.

(20) Matar, S.; Hatch, L. F. *Chemistry of petrochemical processes*; Elsevier, 2001.

(21) Bagger, A.; Ju, W.; Varela, A. S.; Strasser, P.; Rossmeisl, J. Electrochemical CO_2 Reduction: A Classification Problem. *ChemPhysChem* **2017**, *18* (22), 3266−3273.

(22) Umeda, M.; Niitsuma, Y.; Horikawa, T.; Matsuda, S.; Osawa, M. Electrochemical Reduction of CO_2 to Methane on Platinum Catalysts without Overpotentials: Strategies for Improving Conversion Efficiency. *ACS Applied Energy Materials* **2020**, *3* (1), 1119−1127.

(23) Ma, M.; Trześniewski, B. J.; Xie, J.; Smith, W. A. Selective and efficient reduction of carbon dioxide to carbon monoxide on oxide-derived nanostructured silver electrocatalysts. *Angewandte Chemie* **2016**, *128* (33), 9900−9904.

(24) Lu, Q.; Rosen, J.; Jiao, F. Nanostructured Metallic Electrocatalysts for Carbon Dioxide Reduction. *ChemCatChem.* **2015**, *7* (1), 38−47.

(25) Chen, Y.; Li, C. W.; Kanan, M. W. Aqueous CO_2 Reduction at Very Low Overpotential on Oxide-Derived Au Nanoparticles. *J. Am. Chem. Soc.* **2012**, *134* (49), 19969−19972.

(26) Yoo, J. S.; Christensen, R.; Vegge, T.; Nørskov, J. K.; Studt, F. Theoretical Insight into the Trends that Guide the Electrochemical Reduction of Carbon Dioxide to Formic Acid. *ChemSusChem* **2016**, *9* (4), 358−363.

(27) Hori, Y.; Murata, A.; Takahashi, R. Formation of hydrocarbons in the electrochemical reduction of carbon dioxide at a copper electrode in aqueous solution. *Journal of the Chemical Society, Faraday Transactions 1: Physical Chemistry in Condensed Phases* **1989**, *85* (8), 2309−2326.

(28) Kuhl, K. P.; Cave, E. R.; Abram, D. N.; Jaramillo, T. F. New insights into the electrochemical reduction of carbon dioxide on metallic copper surfaces. *Energy Environ. Sci.* **2012**, *5* (5), 7050−7059.

(29) Connors, K. A. *Chemical kinetics: the study of reaction rates in solution*; Wiley-VCH Verlag GmbH, 1990.

(30) Tan, Y. C.; Lee, K. B.; Song, H.; Oh, J. Modulating Local CO_2 Concentration as a General Strategy for Enhancing C−C Coupling in CO_2 Electroreduction. *Joule* **2020**, *4* (5), 1104−1120.

(31) Diamond, L. W.; Akinfiev, N. N. Solubility of CO_2 in water from− 1.5 to 100 C and from 0.1 to 100 MPa: evaluation of literature data and thermodynamic modelling. *Fluid phase equilibria* **2003**, *208* (1-2), 265−290.

(32) Lees, E. W.; Mowbray, B. A. W.; Parlane, F. G. L.; Berlinguette, C. P. Gas diffusion electrodes and membranes for CO_2 reduction electrolysers. *Nature Reviews Materials* **2022**, *7* (1), 55−64.

(33) Ma, W.; He, X.; Wang, W.; Xie, S.; Zhang, Q.; Wang, Y. Electrocatalytic reduction of CO_2 and CO to multi-carbon compounds over Cu-based catalysts. *Chem. Soc. Rev.* **2021**, *50* (23), 12897−12914.

(34) Jouny, M.; Luc, W.; Jiao, F. General Techno-Economic Analysis of CO_2 Electrolysis Systems. *Industrial & Engineering Chemistry Research* **2018**, *57* (6), 2165−2177.

(35) Choi, C.; Kwon, S.; Cheng, T.; Xu, M.; Tieu, P.; Lee, C.; Cai, J.; Lee, H. M.; Pan, X.; Duan, X.; et al. Highly active and stable stepped Cu surface for enhanced electrochemical CO_2 reduction to C_2H_4. *Nature Catalysis* **2020**, *3* (10), 804−812.

(36) Álvarez-Gómez, J. M.; Varela, A. S. Review on Long-Term Stability of Electrochemical CO_2 Reduction. *Energy Fuels* **2023**, *37* (20), 15283−15308.

(37) Nguyen, T. N.; Chen, Z.; Zeraati, A. S.; Shiran, H. S.; Sadaf, S. M.; Kibria, M. G.; Sargent, E. H.; Dinh, C.-T. Catalyst Regeneration via Chemical Oxidation Enables Long-Term Electrochemical Carbon Dioxide Reduction. *J. Am. Chem. Soc.* **2022**, *144* (29), 13254−13265.

(38) Shin, H.; Hansen, K. U.; Jiao, F. Techno-economic assessment of low-temperature carbon dioxide electrolysis. *Nature Sustainability* **2021**, *4* (10), 911−919.

(39) Popović, S.; Smiljanić, M.; Jovanovič, P.; Vavra, J.; Buonsanti, R.; Hodnik, N. Stability and Degradation Mechanisms of Copper-Based Catalysts for Electrochemical CO_2 Reduction. *Angew. Chem., Int. Ed.* **2020**, *59* (35), 14736−14746.

https://doi.org/10.1021/acselectrochem.5c00130
ACS Electrochem. 2025, 1, 2024−2033

(40) Lee, S. Y.; Jung, H.; Kim, N.-K.; Oh, H.-S.; Min, B. K.; Hwang, Y. J. Mixed Copper States in Anodized Cu Electrocatalyst for Stable and Selective Ethylene Production from CO_2 Reduction. *J. Am. Chem. Soc.* **2018**, *140* (28), 8681−8689.
(41) Zhou, Y.; Yao, Y.; Zhao, R.; Wang, X.; Fu, Z.; Wang, D.; Wang, H.; Zhao, L.; Ni, W.; Yang, Z.; et al. Stabilization of Cu+ via Strong Electronic Interaction for Selective and Stable CO_2 Electroreduction. *Angew. Chem., Int. Ed.* **2022**, *61* (31), No. e202205832.
(42) Wu, Y.; Rabiee, H.; Zhao, X. S.; Wang, G.; Jiang, Y. Insights into electrolyte flooding in flexible gas diffusion electrodes for CO_2 electrolysis: from mechanisms to effective mitigation strategies. *Journal of Materials Chemistry A* **2024**, *12* (24), 14206−14228.
(43) Saha, P.; Amanullah, S.; Dey, A. Selectivity in Electrochemical CO_2 Reduction. *Acc. Chem. Res.* **2022**, *55* (2), 134−144.
(44) Yang, K.; Kas, R.; Smith, W. A. In Situ Infrared Spectroscopy Reveals Persistent Alkalinity near Electrode Surfaces during CO_2 Electroreduction. *J. Am. Chem. Soc.* **2019**, *141* (40), 15891−15900.
(45) Varela, A. S. The importance of pH in controlling the selectivity of the electrochemical CO_2 reduction. *Current Opinion in Green and Sustainable Chemistry* **2020**, *26*, No. 100371.
(46) Henckel, D. A.; Counihan, M. J.; Holmes, H. E.; Chen, X.; Nwabara, U. O.; Verma, S.; Rodríguez-López, J.; Kenis, P. J. A.; Gewirth, A. A. Potential Dependence of the Local pH in a CO_2 Reduction Electrolyzer. *ACS Catal.* **2021**, *11* (1), 255−263.
(47) Luo, H.; Chioyama, H.; Thürmer, S.; Ohba, T.; Kanoh, H. Kinetics and Structural Changes in CO_2 Capture of K_2CO_3 under a Moist Condition. *Energy Fuels* **2015**, *29* (7), 4472−4478.
(48) Wu, Y.; Garg, S.; Li, M.; Idros, M. N.; Li, Z.; Lin, R.; Chen, J.; Wang, G.; Rufford, T. E. Effects of microporous layer on electrolyte flooding in gas diffusion electrodes and selectivity of CO_2 electrolysis to CO. *J. Power Sources* **2022**, *522*, No. 230998.
(49) Diercks, J. S.; Pribyl-Kranewitter, B.; Herranz, J.; Chauhan, P.; Faisnel, A.; Schmidt, T. J. An Online Gas Chromatography Cell Setup for Accurate CO_2-Electroreduction Product Quantification. *J. Electrochem. Soc.* **2021**, *168* (6), No. 064504.
(50) Englhard, J.; Bachmann, J. Quantification of CO and Further CO_2 Reduction Products by On-line Mass Spectrometry. *Chemistry−Methods* **2023**, *3* (12), No. e202300019.
(51) Bondue, C. J.; Koper, M. T. M. A DEMS approach for the direct detection of CO formed during electrochemical CO_2 reduction. *Journal of Electroanalytical Chemistry* **2020**, *875*, No. 113842.
(52) Hong, Y.-H.; Zhou, Z.-Y.; Zhan, M.; Wang, Y.-C.; Chen, Y.; Lin, S.-C.; Rauf, M.; Sun, S.-G. Liquid-inlet online electrochemical mass spectrometry for the in operando monitoring of direct ethanol fuel cells. *Electrochemistry Communications* **2018**, *87*, 91−95.
(53) Clark, E. L.; Singh, M. R.; Kwon, Y.; Bell, A. T. Differential Electrochemical Mass Spectrometer Cell Design for Online Quantification of Products Produced during Electrochemical Reduction of CO_2. *Analytical Chemistry* **2015**, *87* (15), 8013−8020.
(54) Ye, K.; Jiang, T.-W.; Jung, H. D.; Shen, P.; Jang, S. M.; Weng, Z.; Back, S.; Cai, W.-B.; Jiang, K. Molecular level insights on the pulsed electrochemical CO_2 reduction. *Nat. Commun.* **2024**, *15* (1), 9781.
(55) Ye, K.; Shen, P.; Xu, M.; Huang, C.; Zhao, L.; Zhou, Z.; Ma, X.-Y.; Cai, W.-B.; Qi, F.; Jiang, K. Real-Time Analysis of CO_2 Reduction Product Distribution by Synchrotron Vacuum Ultraviolet Photoionization Mass Spectrometry. *Analytical Chemistry* **2025**, *97* (7), 3901−3907.
(56) Gautam, M.; Nkurunziza, F.; Muchharla, B.; Kumar, B.; Spurgeon, J. M. Understanding Electrochemical CO_2 Reduction through Differential Electrochemical Mass Spectrometry. *Analytical Chemistry* **2025**, *97* (10), 5372−5392.
(57) Queiroz, A. C.; Souza, M. L.; Camilo, M. R.; Silva, W. O.; Cantane, D. A.; Messias, I.; Pinto, M. R.; Nagao, R.; Lima, F. H. B. Electrochemical Mass Spectrometry: Evolution of the Cell Setup for On-Line Investigation of Products and Screening of Electrocatalysts for Carbon Dioxide Reduction. *ChemElectroChem.* **2022**, *9* (12), No. e202101408.
(58) Mandal, L.; Yang, K. R.; Motapothula, M. R.; Ren, D.; Lobaccaro, P.; Patra, A.; Sherburne, M.; Batista, V. S.; Yeo, B. S.; Ager, J. W.; et al. Investigating the Role of Copper Oxide in Electrochemical CO_2 Reduction in Real Time. *ACS Appl. Mater. Interfaces* **2018**, *10* (10), 8574−8584.
(59) Zhang, G.; Cui, Y.; Kucernak, A. Real-Time In Situ Monitoring of CO_2 Electroreduction in the Liquid and Gas Phases by Coupled Mass Spectrometry and Localized Electrochemistry. *ACS Catal.* **2022**, *12* (10), 6180−6190.
(60) Khanipour, P.; Löffler, M.; Reichert, A. M.; Haase, F. T.; Mayrhofer, K. J. J.; Katsounaros, I. Electrochemical Real-Time Mass Spectrometry (EC-RTMS): Monitoring Electrochemical Reaction Products in Real Time. *Angew. Chem., Int. Ed.* **2019**, *58* (22), 7273−7277.
(61) Hasa, B.; Jouny, M.; Ko, B. H.; Xu, B.; Jiao, F. Flow Electrolyzer Mass Spectrometry with a Gas-Diffusion Electrode Design. *Angew. Chem., Int. Ed.* **2021**, *60* (6), 3277−3282.
(62) Ren, H.; Kovalev, M.; Weng, Z.; Muhamad, M. Z.; Ma, H.; Sheng, Y.; Sun, L.; Wang, J.; Rihm, S.; Yang, W.; et al. Operando proton-transfer-reaction time-of-flight mass spectrometry of carbon dioxide reduction electrocatalysis. *Nature Catalysis* **2022**, *5* (12), 1169−1179.
(63) Parada, W. A.; Mayrhofer, K.; Nikolaienko, P. Real-Time Product Detection during CO_2 Electroreduction on SCILL-Modified Cu Catalysts. *ChemElectroChem.* **2024**, *11*, e202400305.
(64) Zhang, G.; Kucernak, A. Time-Resolved Product Observation for CO_2 Electroreduction Using Synchronised Electrochemistry-Mass Spectrometry with Soft Ionisation (sEC-MS-SI). *Angew. Chem., Int. Ed.* **2023**, *62* (48), No. e202312607.
(65) Rihm, S.; Kovalev, M.; Lapkin, A.; Iii, J.; Kraft, M. On the role of C4 and C5 products in electrochemical CO_2 reduction via copper-based catalysts. *Energy Environ. Sci.* **2023**, *16*, 1697.
(66) Butt, E. N.; Padding, J.; Hartkamp, R. Local Reaction Environment Deviations within Gas Diffusion Electrode Pores for CO_2 Electrolysis. *J. Electrochem. Soc.* **2024**, *171*, 014504.
(67) Li, Y. C.; Yan, Z.; Hitt, J.; Wycisk, R.; Pintauro, P. N.; Mallouk, T. E. Bipolar Membranes Inhibit Product Crossover in CO_2 Electrolysis Cells. *Advanced Sustainable Systems* **2018**, *2* (4), No. 1700187.
(68) Parada, W. A.; Sajevic, U.; Mammadzada, R.; Nikolaienko, P.; Mayrhofer, K. J. J. Tethered Alkylammonium Dications as Electrochemical Interface Modifiers: Chain Length Effect on CO_2 Reduction Selectivity at Industry-Relevant Current Density. *ACS Appl. Mater. Interfaces* **2024**, *16* (23), 30107−30116.
(69) Asnin, L. D. Peak measurement and calibration in chromatographic analysis. *TrAC Trends in Analytical Chemistry* **2016**, *81*, 51−62.
(70) Mermet, J.-M. Calibration in atomic spectrometry: A tutorial review dealing with quality criteria, weighting procedures and possible curvatures. *Spectrochimica Acta Part B: Atomic Spectroscopy* **2010**, *65* (7), 509−523.
(71) Lavagnini, I.; Magno, F. A statistical overview on univariate calibration, inverse regression, and detection limits: Application to gas chromatography/mass spectrometry technique. *Mass Spectrom. Rev.* **2007**, *26* (1), 1−18.
(72) Zhang, R. Probing Liquid Chromatography−Tandem Mass Spectrometry Response Dynamics and Nonlinear Effects for Response Level Defined Calibration Strategies with Simple Methods To Expand Linear Dynamic Ranges. *ACS Omega* **2024**, *9* (1), 607−617.
(73) Trufelli, H.; Palma, P.; Famiglini, G.; Cappiello, A. An overview of matrix effects in liquid chromatography−mass spectrometry. *Mass Spectrom. Rev.* **2011**, *30* (3), 491−509.
(74) Annesley, T. M. Ion Suppression in Mass Spectrometry. *Clinical Chemistry* **2003**, *49* (7), 1041−1044.
(75) Martin, J.; Gracia, A.; Garcia Asuero, A. Fitting Nonlinear Calibration Curves: No Models Perfect. *Journal of Analytical Sciences, Methods and Instrumentation* **2017**, *07*, 1−17.

(76) Galitzine, C.; Egertson, J. D.; Abbatiello, S.; Henderson, C. M.; Pino, L. K.; MacCoss, M.; Hoofnagle, A. N.; Vitek, O. Nonlinear Regression Improves Accuracy of Characterization of Multiplexed Mass Spectrometric Assays. *Molecular & Cellular Proteomics* **2018**, *17* (5), 913−924.
(77) De Mot, B.; Hereijgers, J.; Duarte, M.; Breugelmans, T. Influence of flow and pressure distribution inside a gas diffusion electrode on the performance of a flow-by CO_2 electrolyzer. *Chemical Engineering Journal* **2019**, *378*, No. 122224.
(78) Shin, S.-J.; Choi, H.; Ringe, S.; Won, D. H.; Oh, H.-S.; Kim, D. H.; Lee, T.; Nam, D.-H.; Kim, H.; Choi, C. H. A unifying mechanism for cation effect modulating C1 and C2 productions from CO_2 electroreduction. *Nat. Commun.* **2022**, *13* (1), 5482.
(79) Monteiro, M. C. O.; Dattila, F.; Hagedoorn, B.; García-Muelas, R.; López, N.; Koper, M. T. M. Absence of CO_2 electroreduction on copper, gold and silver electrodes without metal cations in solution. *Nature Catalysis* **2021**, *4* (8), 654−662.
(80) Roberts, F. S.; Kuhl, K. P.; Nilsson, A. High Selectivity for Ethylene from Carbon Dioxide Reduction over Copper Nanocube Electrocatalysts. *Angew. Chem., Int. Ed.* **2015**, *54* (17), 5179−5182.
(81) Piqué, O.; Löffler, M.; Katsounaros, I.; Calle-Vallejo, F. Computational-experimental study of the onset potentials for CO2 reduction on polycrystalline and oxide-derived copper electrodes. *Electrochimica Acta* **2021**, *380*, No. 138247.
(82) Hosseini, S.; Han, S. J.; Arponwichanop, A.; Yonezawa, T.; Kheawhom, S. Ethanol as an electrolyte additive for alkaline zinc-air flow batteries. *Sci. Rep.* **2018**, *8* (1), 11273.
(83) Dinh, C.-T.; Burdyny, T.; Kibria, M. G.; Seifitokaldani, A.; Gabardo, C. M.; García de Arquer, F. P.; Kiani, A.; Edwards, J. P.; De Luna, P.; Bushuyev, O. S.; et al. CO_2 electroreduction to ethylene via hydroxide-mediated copper catalysis at an abrupt interface. *Science* **2018**, *360* (6390), 783−787.

https://doi.org/10.1021/acselectrochem.5c00130
ACS Electrochem. 2025, 1, 2024−2033